

---

This is an electronic reprint of the original article.  
This reprint may differ from the original in pagination and typographic detail.

Basarir, Fevzihan; Al Haj, Yazan; Zou, Fangxin; De, Swarnalok; Nguyen, An; Frey, Alexander; Haider, Ijlal; Sariola, Veikko; Vapaavuori, Jaana

## **Edible and Biodegradable Wearable Capacitive Pressure Sensors: A Paradigm Shift toward Sustainable Electronics with Bio-Based Materials**

*Published in:*  
Advanced Functional Materials

*DOI:*  
[10.1002/adfm.202403268](https://doi.org/10.1002/adfm.202403268)

Published: 25/09/2024

*Document Version*  
Publisher's PDF, also known as Version of record

*Published under the following license:*  
CC BY

*Please cite the original version:*  
Basarir, F., Al Haj, Y., Zou, F., De, S., Nguyen, A., Frey, A., Haider, I., Sariola, V., & Vapaavuori, J. (2024). Edible and Biodegradable Wearable Capacitive Pressure Sensors: A Paradigm Shift toward Sustainable Electronics with Bio-Based Materials. *Advanced Functional Materials*, 34(39), Article 2403268. <https://doi.org/10.1002/adfm.202403268>

---

This material is protected by copyright and other intellectual property rights, and duplication or sale of all or part of any of the repository collections is not permitted, except that material may be duplicated by you for your research use or educational purposes in electronic or print form. You must obtain permission for any other use. Electronic or print copies may not be offered, whether for sale or otherwise to anyone who is not an authorised user.

# Edible and Biodegradable Wearable Capacitive Pressure Sensors: A Paradigm Shift toward Sustainable Electronics with Bio-Based Materials

Fevzihan Basarir, Yazan Al Haj, Fangxin Zou, Swarnalok De, An Nguyen, Alexander Frey, Ijlal Haider, Veikko Sariola, and Jaana Vapaavuori\*

This study presents a significant advancement in sustainable electronics, introducing an innovative capacitive-type wearable pressure sensor crafted entirely from edible and biodegradable biomaterials. The sensor's constituents, encompassing the substrate, electrode, and dielectric elements, are obtained using edible and renewable sources, specifically cellulose and pectin. Leveraging their non-metallic properties, these materials facilitate natural biodegradation, effectively reducing the environmental impact of electronic waste. Employing green chemistry principles during material preparation ensures the exclusion of critical raw materials. The resulting sensors showcase a versatile pressure detection range, from subtle pressures of 100 Pa to a maximum threshold of 100 kPa. Demonstrating a sensitivity of  $0.0294 \text{ kPa}^{-1}$  in the subtle pressure regime, the sensors exhibit a low detection limit of 10 Pa and a fast response time of 118 ms. The sensors exhibited notable repeatability and robustness, enduring over 10 000 loading-unloading cycles without succumbing to fatigue. Applied in real-time human motion detection, the sensors prove their potential applicability. In a biodegradability assessment, all sensor elements exhibit rapid degradation by various fungi, marking a significant stride toward a high-performance, edible, and wearable capacitive pressure sensor that can be deposited as biowaste at the end of its lifecycle.

vital signs, enabling healthcare professionals to gather accurate and reliable data. For instance, by monitoring pressure, healthcare providers can assess various physiological parameters, such as heart rate, wrist pulse, and muscle and joint activities. Wearable pressure sensors offer the advantage of non-invasiveness and convenience, allowing patients to go about their daily activities, while still being monitored.<sup>[1]</sup> Past research efforts have brought forth wearable pressure sensors founded on capacitive,<sup>[2]</sup> piezoresistive,<sup>[3]</sup> piezoelectric,<sup>[4]</sup> triboelectric,<sup>[5]</sup> and optical<sup>[6]</sup> sensing mechanisms. Among these, capacitive sensors have ascended as a preferred alternative, attributed to their simplistic design, enhanced precision, lower power requirements, and lesser dependency on external factors like temperature and humidity.<sup>[2]</sup> In comparison to other technologies, capacitive pressure sensors offer superior performance, characterized by low hysteresis, exceptional accuracy, and high measurement reliability. Notably, they demonstrate remarkable robustness, withstanding harsh operating

conditions owing to their simple mechanical design. Their inherent resistance to electromagnetic interference (EMI) makes them well-suited for operation in electrically noisy environments.<sup>[7,8]</sup>

Customarily, flexible capacitive sensors are composed of two key parts: a flexible dielectric layer sandwiched between two

## 1. Introduction

Wearable pressure sensors play a crucial role in healthcare monitoring, offering numerous benefits and improving patient care. These sensors provide real-time and continuous monitoring of

F. Basarir, Y. A. Haj, F. Zou, S. De, J. Vapaavuori  
Department of Chemistry and Materials Science  
Aalto University  
P.O. Box 16100, AALTO FI-00076, Finland  
E-mail: [jaana.vapaavuori@aalto.fi](mailto:jaana.vapaavuori@aalto.fi)

 The ORCID identification number(s) for the author(s) of this article can be found under <https://doi.org/10.1002/adfm.202403268>

© 2024 The Author(s). Advanced Functional Materials published by Wiley-VCH GmbH. This is an open access article under the terms of the [Creative Commons Attribution](https://creativecommons.org/licenses/by/4.0/) License, which permits use, distribution and reproduction in any medium, provided the original work is properly cited.

DOI: 10.1002/adfm.202403268

A. Nguyen, A. Frey  
Department of Bioproducts and Biosystems  
Aalto University  
P.O. Box 16100, AALTO FI-00076, Finland  
I. Haider, V. Sariola  
Faculty of Medicine and Health Technology  
Tampere University  
Korkeakoulunkatu 3, Tampere 33720, Finland

flexible electrodes. Upon the application of pressure on the sensor, the dielectric layer contracts in thickness, which in turn leads to an increase in the capacitance value. Flexible pressure sensors, with the ability to measure a broad range of pressures from subtle (1 Pa–1 kPa), low (1–10 kPa), to medium pressures (10–100 kPa), have proved valuable in applications such as human motion detection, healthcare monitoring, and human-machine interfaces.<sup>[9,10]</sup>

Common flexible substrates used in capacitive sensors encompass polymer films like polydimethylsiloxane (PDMS),<sup>[11]</sup> Ecoflex,<sup>[12]</sup> polyester (PET),<sup>[13]</sup> polyurethane (PU),<sup>[14]</sup> poly(vinylidene fluoride) (PVDF),<sup>[15]</sup> and polyvinyl alcohol (PVA).<sup>[16]</sup> To develop flexible electrodes, solution-processable nanomaterials, including carbon nanotubes,<sup>[17]</sup> graphene,<sup>[18]</sup> Mxenes,<sup>[19]</sup> and silver nanowires (AgNWs),<sup>[10]</sup> are frequently coated or printed onto these polymer films. Considering dielectric layer of the sensors, PDMS,<sup>[20]</sup> Ecoflex<sup>TM</sup>,<sup>[21]</sup> polyvinylidene fluoride,<sup>[22]</sup> polyimide,<sup>[23]</sup> and polymethyl methacrylate<sup>[24]</sup> have been extensively used in flexible devices. Nevertheless, to augment the sensor performance, structural modifications of the polymer dielectric materials are occasionally mandated. The introduction of porosity into the dielectric layer has surfaced as a leading research direction for increasing sensitivity. The integration of porosity facilitates easier deformation of the dielectric layer due to a lower Young's modulus, thereby improving the effective dielectric constant and enhancing sensitivity.<sup>[2,9]</sup>

However, the abovementioned widespread material choices pose significant environmental concerns due to non-biodegradability and complex, hazardous chemical manufacturing processes, leading to substantial electronic waste and environmental pollution. It is important to highlight that in 2019, the global generation of electronic waste (e-waste) amounted to 53.6 million metric tons (Mt), with only 17.4% of this quantity being officially recorded as appropriately gathered and recycled.<sup>[25]</sup> Consequently, biodegradable electronics have garnered significant interest from both the scientific community and industry, owing to the pressing issues associated with environmental pollution and the recyclability of waste.<sup>[26]</sup> Numerous research groups have endeavored to create biodegradable capacitive pressure sensors, with a primary focus on the development of biodegradable electrodes and dielectric materials.<sup>[27–33]</sup> To date, materials such as thermally evaporated magnesium<sup>[27]</sup> and zinc,<sup>[33]</sup> alongside solution-processed copper<sup>[32]</sup> and silver nanowires,<sup>[31]</sup> have been employed as electrode materials. Substrates like polyhydroxybutyrate/polyhydroxyvalerate (PHB:PHV),<sup>[27]</sup> polylactic acid (PLA),<sup>[33]</sup> polyvinyl alcohol (PVA),<sup>[29]</sup> silk,<sup>[30]</sup> tree leaf,<sup>[31]</sup> and chitosan<sup>[32]</sup> films/sheets have undergone thorough investigation. Furthermore, the application of biodegradable dielectric materials, including poly(glycerol sebacate) (PGS) film,<sup>[27]</sup> polylactic-co-glycolic acid/polycaprolactone (PLGA:PCL) nanofiber mat,<sup>[29]</sup> rose petal film,<sup>[31]</sup> and chitosan sheets,<sup>[32]</sup> has been explored. Typically, the biodegradability of these sensors has been assessed through incubation in phosphate-buffered saline (PBS) solution. However, the claim of complete biodegradability remains uncertain, as the presence of undegraded residues post-testing poses new challenges in waste disposal.

On the other hand, emerging domain of edible electronics focuses on creating digestible devices exclusively from food ingredients and additives, offering solutions to several limitations in-

herent in current ingestible electronic devices. This field is anticipated to significantly impact gastrointestinal monitoring, therapeutic interventions, and rapid assessment of food quality.<sup>[34]</sup> Notably, Kim et al. have developed an electrochemical sensor capable of detecting small biologically relevant molecules such as catechol, uric acid, ascorbic acid, dopamine, and acetaminophen.<sup>[35]</sup> Further advancements include Wu et al.'s creation of an edible pH sensor, a radio frequency filter, and a microphone.<sup>[36]</sup> More recent developments by Caironi and colleagues include an edible battery,<sup>[34]</sup> self-powered edible defrosting sensor,<sup>[37]</sup> edible pill designed for intrabody communication,<sup>[38]</sup> and edible strain sensor.<sup>[39]</sup> These instances of edible sensors and active electrical components in the edible electronics field are highly promising for the development of more complex edible electronic systems, such as pressure sensors.

In response to these issues, in this work, we have developed a sustainable, environmentally friendly, and edible alternative in the form of a biomass-based and biodegradable wearable pressure sensor. The sensor components, including the substrate, electrode, and dielectric materials, were fabricated using fully renewable and edible resources, which possess the ability to naturally degrade over time, thereby minimizing the environmental impact associated with electronic waste. Importantly, the preparation of these materials adhered to green chemistry principles, ensuring that no toxic chemicals were utilized during the fabrication process. Following thorough characterization of the sensor's properties, its applicability was demonstrated in human motion detection.

## 2. Results and Discussion

### 2.1. Characterization of the Electrode

The formulation of the electrically conductive paste was done exclusively using biomass-derived and edible materials without adverse toxic effects, namely carnauba wax, vegetable oil, and carbonized cellulose cryogel particles. The edibility of the materials was discussed in detail in the Supporting Information. Briefly, the results confirm the biocompatible and edible nature of the sensor component materials. Pectin, carnauba wax, and canola oil are all common food additives approved by regulatory bodies such as FDA and EFSA. The cellulose sheets, though not directly consumed in our diet, find parallels in various approved cellulose-based food additives and edible coatings. While pure carbon is not digestible, its use aligns with the safety standards set for activated carbon in food products. These findings support the overall edibility of the developed wearable pressure sensor.

The wax and oil were combined through a melting process, after which the requisite quantity of carbon particles (10% w/w of wax+oil) was incorporated. This method avoided the use of solvents and needed a process temperature of 100 °C, thereby ensuring a sustainable and uncomplicated procedure. The introduction of conductive materials into insulating matrices effectively triggers the onset of electrical conductivity in the resultant composites. The minimal filler loading necessary to induce the transition of the composite from an insulator to a conductor is denoted as the electrical percolation threshold. The resistance of the carbon paste was evaluated in relation to the mass of the carbon particle filler incorporated within the wax-oil matrix and

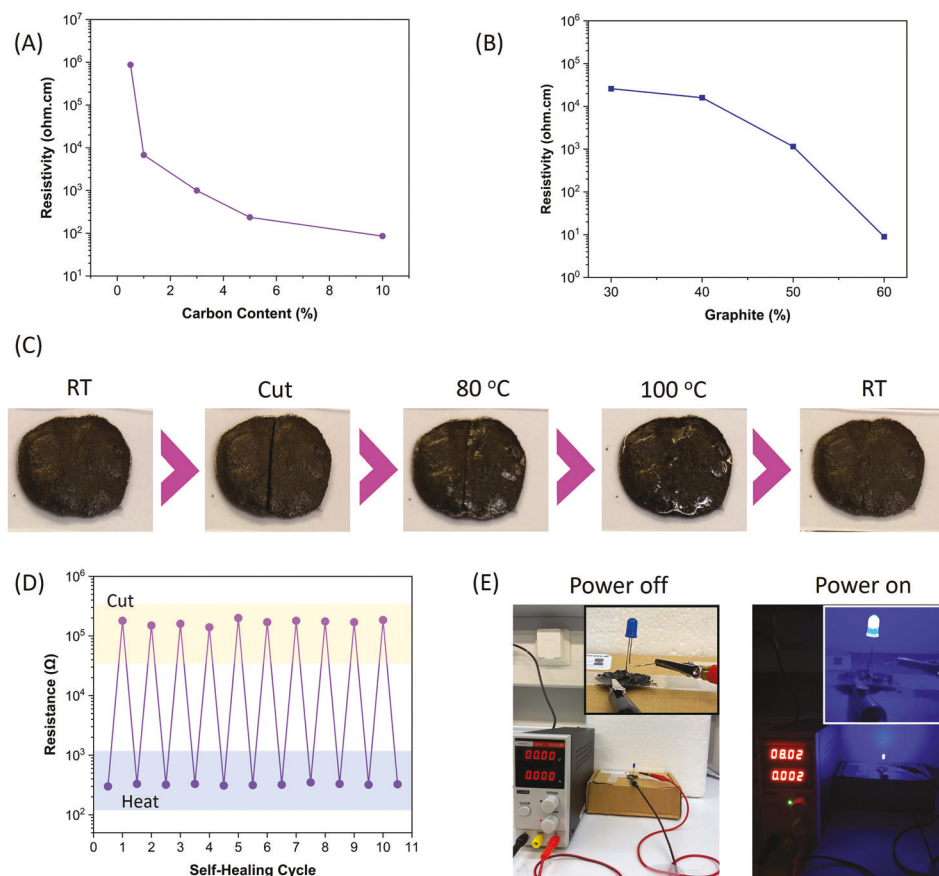


**Figure 1.** A) Influence of carbon cryogel content on the resistivity of the electrode, B) Effect of graphite content on the resistivity of the electrode, C) Digital images of self-healing property of the carbon cryogel paste, D) Resistance change of carbon cryogel paste with repeated cutting and heating, and E) Powering a blue LED through the application of voltage using the carbon paste.

subsequently converted into resistivity. At a carbon content of 1%, electrical percolation was achieved, leading to a decrease in resistivity to  $<10 \text{ k}\Omega\text{-cm}$  (Figure 1A). Increasing the filler content to 10% allows resistivity to reach values as low as  $85 \text{ }\Omega\text{-cm}$ . However, it is worth noting that a carbon content above 10% prevents proper film formation.

For comparative purposes, graphite was used as the conductive filler. As illustrated in Figure 1B, the transition from insulator to conductor occurs at a graphite content of 40%, with resistivity values falling to 1150 and  $9 \text{ }\Omega\text{-cm}$  at 50% and 60% loading, respectively. Significantly, a graphite content of 60% led to suboptimal film formation. It can be observed that the paste containing 10% carbon cryogel exhibits a lower resistivity of  $85 \text{ }\Omega\text{-cm}$ , in contrast to the paste with 50% graphite content, that demonstrates a higher resistivity of  $1150 \text{ }\Omega\text{-cm}$ . This difference can be attributed to low density and high surface specific area of carbon cryogel particles, as shown in Figure S1 (Supporting Information). In addition, 2-point probe I-V measurements were performed, and the results were presented in Figure S2 (Supporting Information). Notably, the carbon paste containing 0.5 wt% carbon aerogel particles exhibited non-ohmic behavior, whereas pastes containing 1 and 10 wt% displayed ohmic behavior. These findings support our previous conclusion that the percolation threshold for electrical conductivity lies between 0.5–1 wt% car-

bon aerogel particle concentration. The resistivity values acquired align with other studies that use activated carbon solely as the filler (resistivity range of  $0.5\text{--}1000 \text{ }\Omega\text{-cm}$ ),<sup>[40–42]</sup> but here with the additional benefits characteristic of a paste, such as malleability, adaptability, and compatibility with large-scale production techniques.

The use of a non-drying vegetable oil in the paste is anticipated to facilitate the coating due to enhanced fluidity, which is also predicted to confer thermal healing properties to the paste. As demonstrated in Figure 1C, the paste, when cut with a blade, exhibited a significant loss in conductivity. However, heating the paste to  $100 \text{ }^\circ\text{C}$  allowed the liquefied paste to flow into the damaged region, effectively repairing it. Upon returning to room temperature, the scratches were remedied, and the conductivity reinstated (Figure 1D). It was observed that even after ten such cycles, the damage was rectified by this heating and cooling cycle. These observations affirm the thermal healing property of the conductive paste, which can repair scratches by undergoing a transition from liquid to solid state with heating and cooling, respectively. It is crucial to note that the resistance values were measured with square samples ( $2.5 \text{ cm} \times 2.5 \text{ cm}$ ) to eliminate the shape effect. Additionally, the electrical resistivity of the paste, with a 10% carbon filler concentration, is adequately low to power a light-emitting diode (LED), as shown in Figure 1E.

## 2.2. Characterization of the Sensors

The sensor design is detailed in **Figure 2A**, where a porous pectin xerogel is positioned between two cellulose substrates, with the carbon paste-coated side oriented toward the xerogel. The cellulose substrate, carbon paste film, and pectin xerogel in the study possess respective thicknesses of  $200 \pm 10 \mu\text{m}$ ,  $100 \pm 8 \mu\text{m}$ , and  $1 \pm 0.05 \text{ mm}$ . It is crucial to emphasize that the selection of materials for the sensor construction exclusively involved edible substances, ensuring no detrimental impact on human health. The edibility of these materials is further elaborated upon in the Supporting Information section under “Edibility of the Materials”. The surface of the pectin xerogel exhibited aligned porous morphology (**Figure 2B**), whereas the cross-sectional view revealed an accordion like structure as shown in **Figure 2C**, which is comparable to our previous work.<sup>[43]</sup> The suitability of the pectin xerogel for pressure sensor applications hinges on its mechanical properties, particularly its elastic modulus. The xerogel’s porous structure and low elastic modulus of 10 kPa (1% tangent modulus) translate to significant compressibility. This characteristic allows the material to deform under external pressure (as demonstrated in **Figure S3**, Supporting Information) and subsequently recover to its original form. This combination of compressibility and recoverability suggests the potential of the pectin xerogel for achieving precise and reliable pressure measurements. On the other hand, the cellulose nanofiber (CNF) substrate exhibited a uniform and smooth macro structure, as evidenced in **Figure 2D**. Upon examination at greater magnification, the film revealed a nonporous and microfibrillar microstructure, as detailed in **Figure 2E**, which can be attributed to the proper filtration and hot-press processing of CNF. **Figure 2F** presents the macroscopic morphology of the cellulose substrate coated with carbon paste. The image reveals a coating that is not entirely smooth, displaying slight roughness. Upon closer inspection at higher magnification, it is evident that the carbon cryogel particles are uniformly distributed throughout the paste, exhibiting no evidence of segregation, as depicted in **Figure 2G**. Morphology of the carbon cryogel particles was characterized by SEM, as shown in **Figure S4** (Supporting Information).

A thorough evaluation of the sensor performance was conducted under varying pressure conditions, extending from 0.1 to 100 kPa. This range is representative of the typical pressure experienced by human skin in daily activities.<sup>[44]</sup> A mechanical tester, furnished with a 12.8 mm diameter cylindrical probe, was employed to apply pressure to the sensor in a progressive manner. The imposition of a compressive force onto the sensor prompts a decrease in the gap between the two parallel electrodes, subsequently resulting in a rise in capacitance. Additionally, during the application of compressive forces, the air within the pore network of the system is expelled and replaced by the surrounding pectin framework. Under applied pressure, the accordion-like structure compresses, leading to the formation of a multilayered pectin sheet morphology, as evidenced in **Figure S5** (Supporting Information). Thus, along with the reduced electrode separation, permittivity of the dielectric layer is increased, when air is replaced by pectin, with a higher relative permittivity.

Initially, the sensor’s repetitive response to a 5 kPa pressure was examined, as depicted in **Figure 3A**. The capacitance displayed consistent signals with the applied pressure throughout

five successive loading and unloading cycles. The sensor was further tested under a range of pressures, extending from 0.1 kPa to 100 kPa, as demonstrated in **Figure 3B**. An upward trend in capacitance was noted with increasing pressure, a phenomenon attributable to the pressure-induced thickness reduction and an increase in relative permittivity. In the subtle (100 Pa–1 kPa), low (1 kPa–10 kPa), and moderate pressure domains (10 kPa – 100 kPa), the sensor showcased sensitivities of 0.0294, 0.0204, and  $0.0009 \text{ kPa}^{-1}$ , respectively (**Figure 3C**).

The sensitivity  $S$  of the sensor was calculated according to the following formula.<sup>[31]</sup>

$$S = \frac{d(C/C_0)}{dP} \quad (1)$$

where  $C$  is the capacitance,  $C_0$  is the initial capacitance, and  $P$  is the applied pressure.

The detailed graphs for sensitivity calculations in different pressure regimes are demonstrated in **Figure S6** (Supporting Information). It is worthy to note that the capacitance change and sensitivity reduced dramatically beyond 10 kPa. This can be attributed to the mechanical properties of the pectin xerogel. As illustrated in **Figure S3** (Supporting Information), the xerogel exhibits a classic linear-plateau-like densification behavior, commonly observed in polymeric foams.<sup>[45]</sup> This translates to a significant compression strain reaching  $\approx 60\%$  at 10 kPa, with minimal further strain increase under higher stress. Consequently, the reduced sensitivity at pressures exceeding 10 kPa can be ascribed to the densification of the pectin xerogel. This densification process likely leads to the formation of a multilayered pectin sheet morphology, as observed in **Figure S5** (Supporting Information).

The sensor response and recovery times were examined by loading and sustaining a pressure of 100 Pa for a 5 s duration, as illustrated in **Figure 3D**. The sensor quickly displayed an elevation in capacitance, demonstrating a brisk response time of 118 ms, slightly exceeding the response time of the human skin (30–50 ms).<sup>[46]</sup> Upon removal of pressure, the sensor promptly exhibited a decrease in capacitance with a minimal recovery period of  $\approx 130 \text{ ms}$ , gradually reverting to its initial value. The durability of the sensor was assessed via 10000 loading/unloading cycles at a pressure of 5 kPa, revealing its resilience and consistent functionality without significant signs of fatigue (**Figure 3E**).

**Table 1** demonstrates a comparative analysis of various biodegradable capacitive pressure sensors, including the work presented in this study. In the realm of biodegradable capacitive pressure sensors, the study at hand, utilizing a carbon paste electrode, cellulose substrate, and pectin xerogel dielectric, demonstrates a commendable balance in performance metrics. Our sensor exhibits a moderate sensitivity of  $0.0294 \text{ kPa}^{-1}$  in a focused pressure range of 0.1–1 kPa, and a notably quick response time of 118 ms, positioning it well for applications requiring the detection of subtle pressures. When compared with other studies in the field, such as those using magnesium (Mg) and zinc (Zn) films as well as silver (Ag) and copper (Cu) nanowire-based electrodes, a variation in performance becomes evident. Sensors demonstrated by Bao research group,<sup>[27,28]</sup> for instance, show a higher sensitivity than ours but at a similar or slightly expanded pressure range. The higher sensitivity could be attributed to the introduced microstructures in the dielectric layer. In particular,

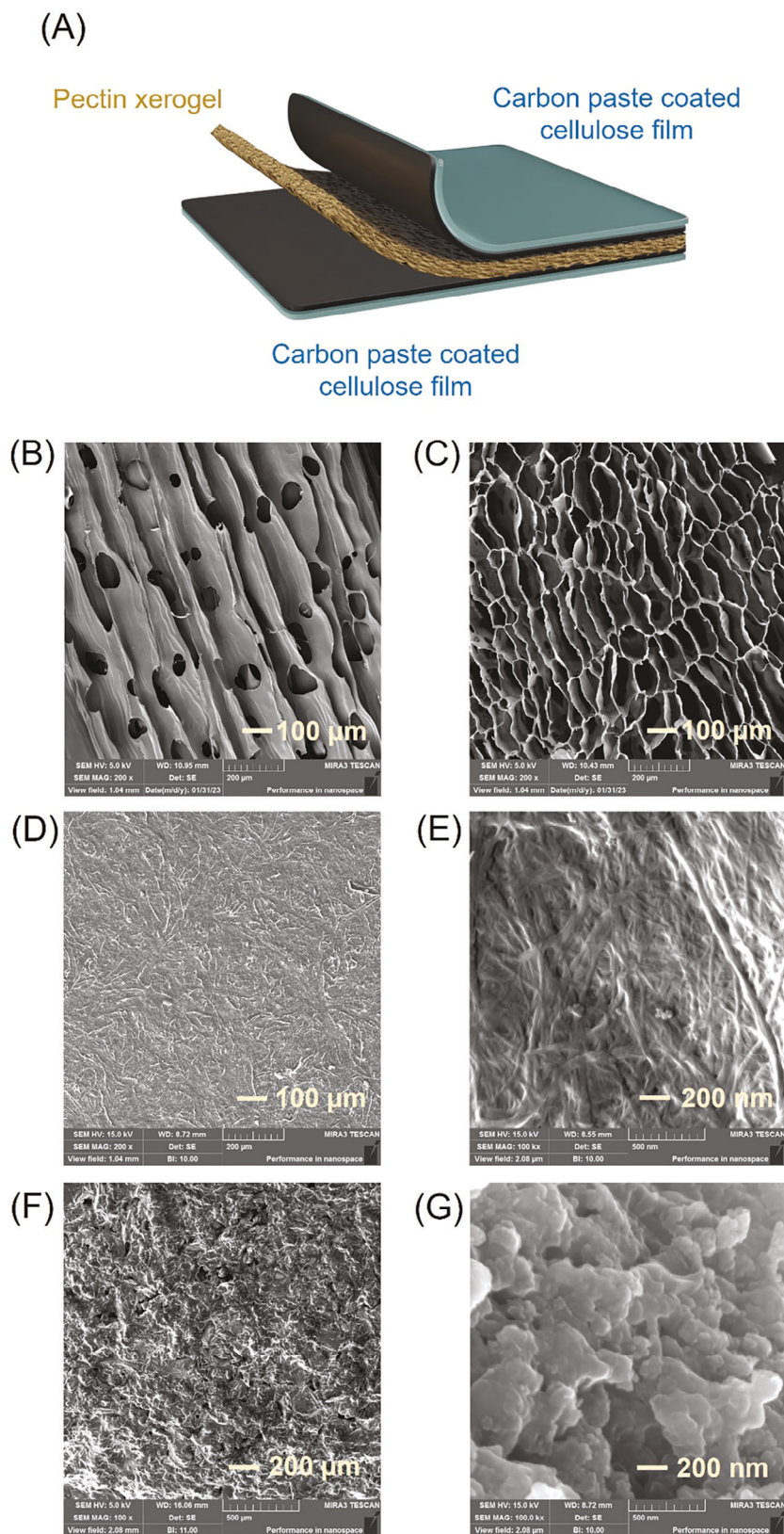


**Figure 2.** A) Schematic demonstration of sensor structure, SEM images of B) Surface and C) Cross section of pectin xerogel dielectric layer, cellulose substrate D) 200x magnification, E) 100 000x magnification and carbon cryogel paste film on cellulose substrate F) 100x magnification and G) 100 000x magnification.

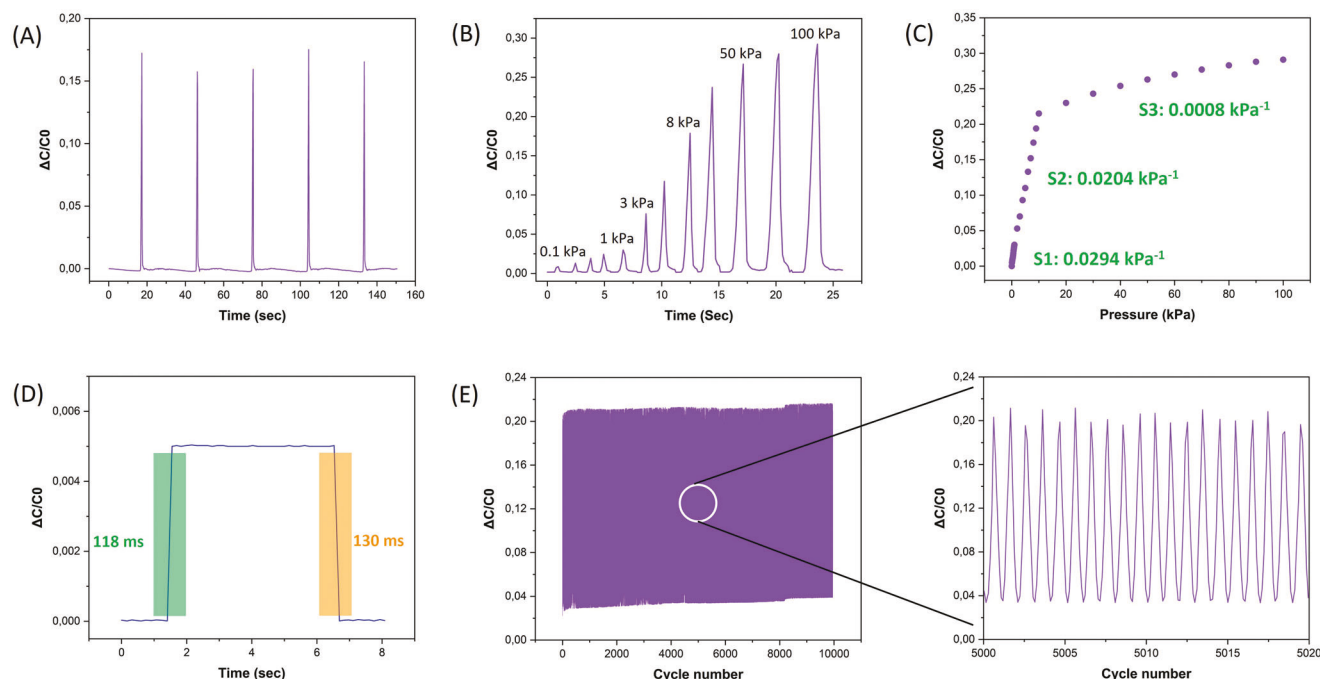


**Figure 3.** Properties of the pressure sensor. A) Repeated responses of the sensor to 5 kPa pressure, (B) real-time responses of the sensor to various pressure, C) Sensitivity of sensor in different pressure regimes, D) Response and recovery time of sensor, and E) Stability of the sensor tested for 10 000 cycles under an applied pressure of 5 kPa.

the sensor exhibited by Song et al. stands out with the highest sensitivity of  $1.7 \text{ kPa}^{-1}$  and a broader pressure range of 0–5 kPa, albeit with a slower response time. On the other end of the spectrum, the sensor shown by Hou,<sup>[30]</sup> while covering an extensive pressure range of 0–45 kPa, offers a lower sensitivity than our design. This comparative analysis underscores the diversity in sensor performance across different material compositions, revealing a trade-off between sensitivity, pressure range, and response time that guides their suitability for various applications.

### 2.3. Human Motion Detection

The sensor displayed several advantageous characteristics, such as the ability to detect varying pressure ranges, moderate sensitivity, a lightweight and flexible structure, rendering it an apt choice for human motion tracking. Its potential applications were demonstrated by attaching it to different body parts, including

the wrist, bicep, finger joint, face, and under the foot, with real-time monitoring of changes in capacitance during specific movements. The set-up for the pressure sensing and the wearable sensing is depicted in detail in Figure S7 (Supporting Information). Initially, the sensor was placed under the shoe to observe pressure fluctuations during jumping activities, as depicted in Figure 4A. Throughout the jumping motions, the sensor provided consistent and repeatable signals, highlighting its remarkable stability under pressure. Additionally, when mounted on the wrist, as shown in Figure 4B, wrist bending of  $90^\circ$  led to an increase in capacitance, which reverted to the baseline upon returning to the starting position.

The sensor response to the bicep muscle contraction and relaxation was marked by an increase in capacitance, reflecting the pressure applied due to muscle movement. This response was clearly demonstrated in Figure 4C, with consistent readings observed across repeated actions. Similarly, when applied to the index finger joint, the sensor successfully detected

**Table 1.** Performance comparison of the biodegradable capacitive pressure sensors.

Electrode material	Substrate	Dielectric material	Max. sensitivity [ $\text{kPa}^{-1}$ ]	Pressure range [kPa]	Response time [ms]	Biodegradability test	Ref.
Carbon paste	Cellulose	Pectin xerogel	0.0294	0.1-1	118	Fungi	This work
Mg	PHB/PHV	PGS	0.76	0-2	–	PBS solution	[27]
Mg	PLA	PGS	0.70	0-1	–	PBS solution	[28]
Zn	PVA	PLGA:PCL nanofiber	0.888	0-2	251	PBS solution	[29]
Silver	Silk	Silicone rubber	0.01887	0-45	–	Enzyme	[30]
Silver nanowires	Tree leaf	Rose petal	0.08	0-1	–	PBS solution	[31]
Copper nanowires	Chitosan	Glycerine: Chitosan	1.7	0-5	180	Enzyme	[32]

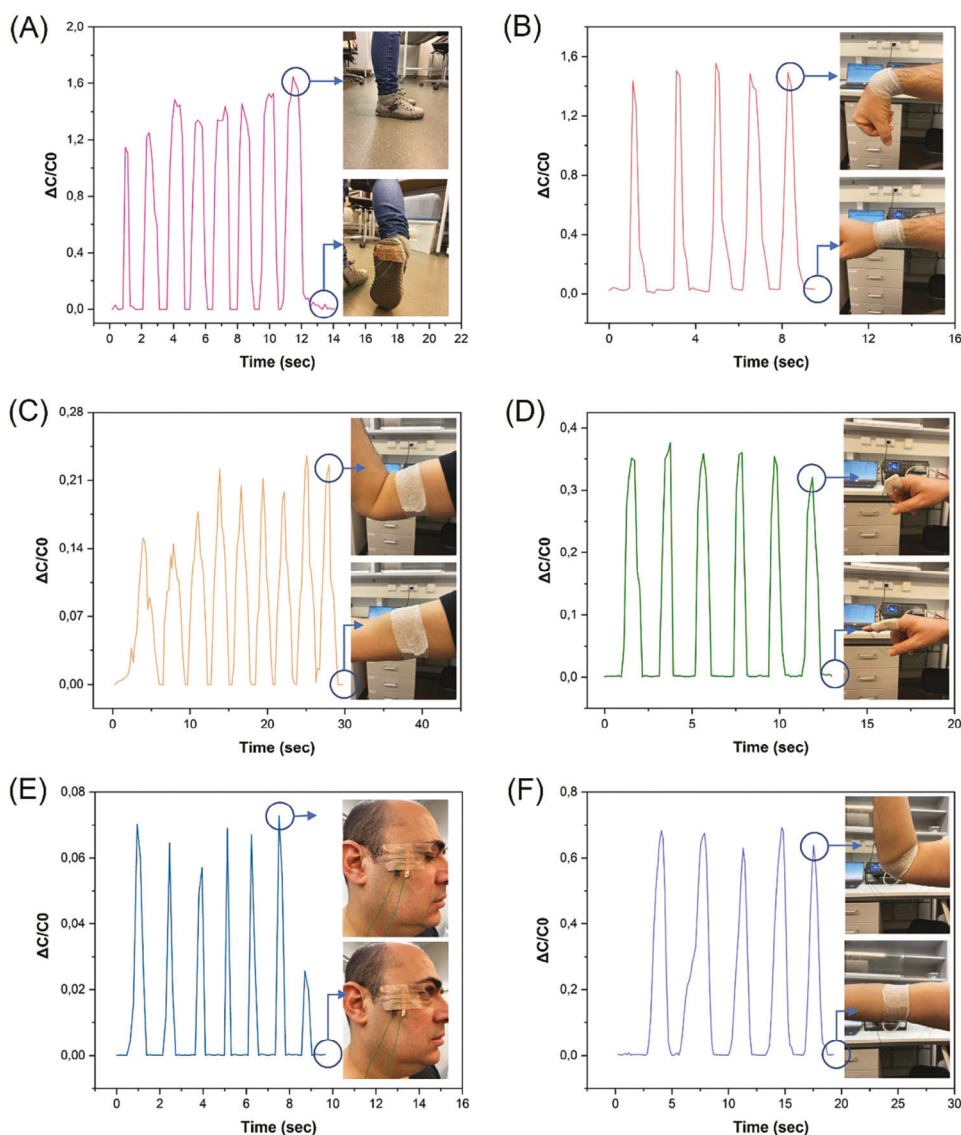


**Figure 4.** Real-time monitoring of human motion A) Jumping, B) Wrist bending, C) Relaxed and fully inflated bicep, D) Finger joint bending, E) Eye blinking, and F) Elbow bending.

bending movements, causing an increase in capacitance, as shown in Figure 4D. This detection yielded reliable and repeatable outcomes during the finger's bending and unbending cycles. Furthermore, the sensor was attached to the facial muscles controlling eye blinking, registering immediate responses to blinking, as shown in Figure 4E, with capacitance reverting to its original state upon muscle relaxation.

Ultimately, upon positioning the sensor on the elbow joint to monitor arm bending, it demonstrated a consistent return to its initial capacitance following each flexion cycle. This behavior illustrates the sensor's ability to produce highly repeatable signals and maintain remarkable stability throughout the process of continuous 90-degree arm flexion and subsequent relaxation, as shown in Figure 4F.

Additionally, to evaluate the long-term stability of the sensors, their response to finger and wrist bending was moni-

tored. The results are presented in Figure S8 (Supporting Information). As can be seen in this Figure, the sensors maintained consistent signal output during continuous bending and unbending cycles of the wrist and finger for 30 and 15 min, respectively.

While the human motions shown in Figure 4 primarily involve compressional deformation, real-world scenarios might encompass additional deformation modes such as stretching, shearing, and others, collectively referred to as multimodal deformation. To isolate the sensor's response to a specific deformation mode, we investigated its behavior under uniaxial compression by applying finger pressure directly onto the sensor surface as shown in Figure S9 (Supporting Information). A noteworthy observation is the positive correlation between finger pressing level and capacitance change. In other words, as the applied finger pressure increases, the magnitude of the capacitance change also increases.

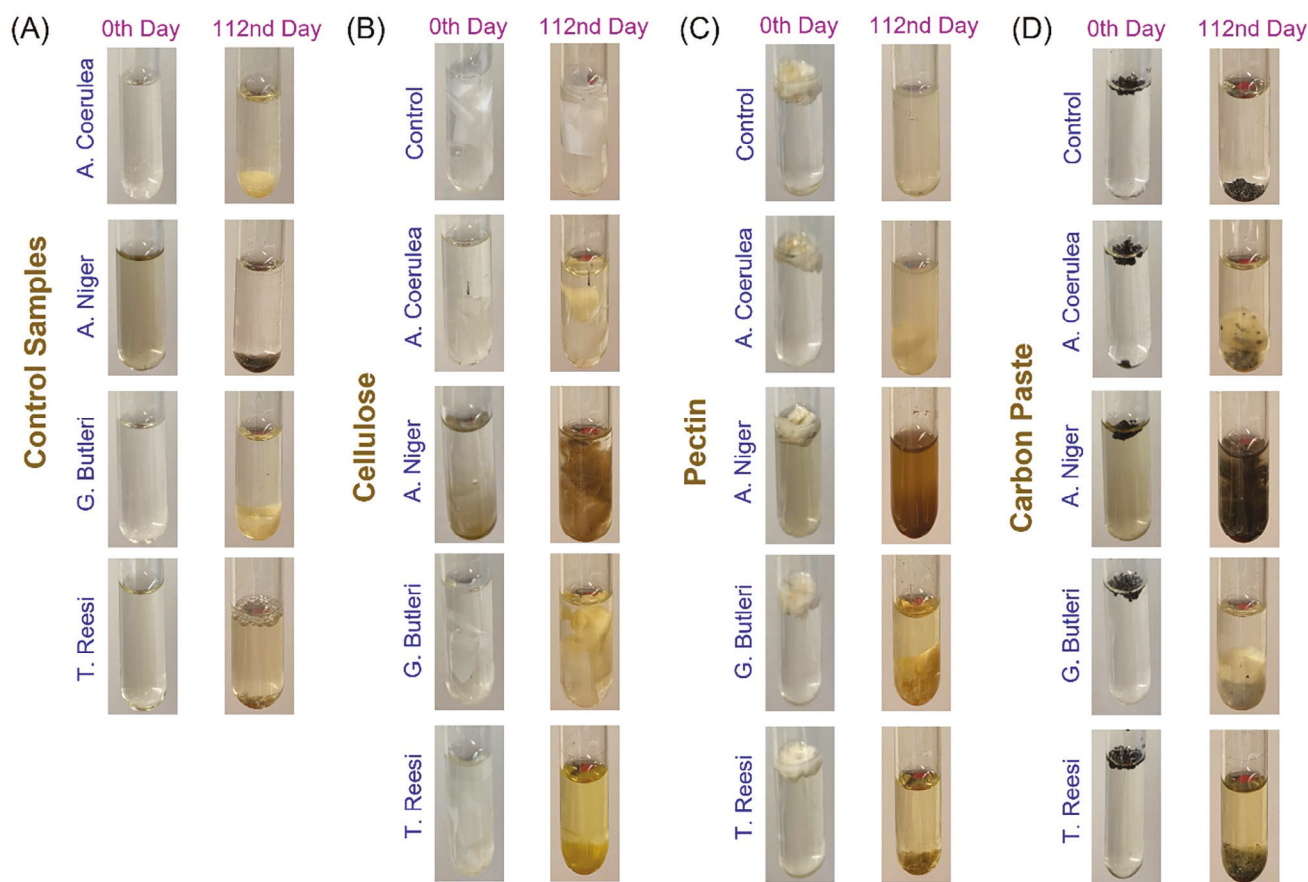


**Figure 5.** Visual biodegradability assessment of A) Control samples, B) Cellulose, C) Pectin, and D) Carbon paste.

To evaluate the pressure response of the sensor during real-time human motion monitoring, the measured capacitance changes were compared to the pressure response curve presented in Figure 3C. Notably, activities such as jumping, elbow bending, and wrist bending generated pressure exceeding 100 kPa within each cycle. Conversely, eye blinking, bicep muscle contraction, and finger joint bending produced pressure values of  $\approx 1$ , 10, and 100 kPa per cycle, respectively.

## 2.4. Biodegradability Assessment

The experimental medium utilized was Yeast Nitrogen Base (YNB) without any amino acids and glucose. Theoretically, the absence of carbon sources in this medium is expected to inhibit significant fungal proliferation. This experimental design was intended to assess the capability of the fungi to decompose the test material into utilizable carbon sources. Substantial fungal growth in conjunction with the depletion of the test materials would indicate the capacity of the fungi to degrade these materials, thereby affirming their biodegradability. It is important to note that in the control samples, which only contained fungal spores and YNB medium, fungal growth was observed, as depicted in Figure 5A (Detailed analysis could be found in Figure S10, Supporting Information) This growth can be attributed to the presence of glucose (2% w/v) in the spore storage solution. Therefore, when

these spore solutions were added to the YNB medium, a limited quantity of glucose was made available, enabling fungal growth.

In this study, we noted that carbon cryogel paste and cellulose substrate remained undissolved in Yeast Nitrogen Base (YNB) medium, whereas pectin dissolved within 7 days, resulting in a turbid solution, as observed in the material control samples (Figures S11–S13, Supporting Information). The degradation of the tested materials is primarily attributed to the enzymatic activity of the fungi during their growth phase. *T. Reesei* has been a leading source for the production of cellulases – enzymes that specifically target cellulose to generate glucose—for over seventy years.<sup>[47,48]</sup> Hence, it was not surprising that *T. reesei* was the most effective fungus in degrading cellulose in our experiment (Figure 5B). *A. Niger*, known to secrete cellulases as evidenced by both enzyme assays and genomic analysis, exhibits less efficient growth when solely relying on cellulose as a carbon source (Detailed analysis in Figure S11, Supporting Information).<sup>[49,50]</sup> This may be linked to the variations in the types of cellulases produced by *A. niger* compared to *T. reesei*.<sup>[51]</sup> Despite there is evidence indicating the secretion of cellulases by *G. butleri*, our result showed that the fungus did not degrade cellulose in minimal medium with cellulose as the sole carbon source.<sup>[52]</sup> This is likely due to the composition of the cellulases secreted by *G. butleri*, as the phenomenon is also seen in *A. niger* as mentioned above. No previous study can be found related to the production of cellulase by *A. coerulea*.

The enzymatic breakdown of pectin is mediated by the enzyme pectinase. *A. Niger* has been identified as a leading organism for pectinase production, a conclusion supported by both fermentation techniques and genomic analyses (Figure 5C).<sup>[53–55]</sup> In contrast, *T. Reesei* is known to possess an incomplete set of enzymes necessary for pectin degradation, accounting for its slower rate of pectin breakdown (Detailed analysis Figure S12, Supporting Information). To date, there has been no research exploring the capabilities of *G. Butleri* and *A. Coerulea* in pectin degradation.<sup>[56]</sup> Our findings suggest that *G. Butleri* could serve as an alternative to *A. Niger* for pectin breakdown, given its demonstrated efficiency in degrading pectin in a minimal medium environment.

Additionally, we explored the biodegradability of carbon paste with the same fungi. The composition of the carbon paste included carbon cryogel particles, canola oil, and carnauba wax. *A. Coerulea* and *G. Butleri* exhibited limited growth, while *T. Reesei* showed no significant degradation of the carbon paste. *A. Niger*, however, displayed the most pronounced biodegradation capabilities. Nonetheless, at the conclusion of a 16-week period, residual carbon cryogel particles were still detectable (Detailed analysis Figure S13, Supporting Information). Although there are limited studies in the literature, existing ones confirm the biodegradability of canola oil<sup>[57]</sup> and carnauba wax<sup>[58]</sup> by fungi. The observed fungal growth in the mediums containing *A. Coerulea*, *G. Butleri* and *A. Niger* could be attributed to the decomposition of the canola oil and carnauba wax, leaving behind carbon cryogel particles as the residual waste.

As shown in Table 1, the biodegradability tests conducted in this work and the tests for the other biodegradable sensors in the literature demonstrate the diverse methodologies employed in assessing the degradation of materials through biological means. In our study, the focus was on utilizing fungi as a primary agent for biodegradation. We believe this approach presents a unique perspective compared to the previous works, where phosphate-buffered saline (PBS) solution was predominantly used.<sup>[27–29,31]</sup> The utilization of fungi in our work offers insights into a more natural and environmentally relevant biodegradation process since the fungi are known for their robust enzymatic systems capable of breaking down complex materials, which could potentially offer a more comprehensive understanding of the biodegradability of materials in real-world conditions. Besides, the references that employed PBS solution as the biodegradability testing medium primarily mimic a controlled, physiological environment. This approach is beneficial for understanding the degradation process in conditions that resemble biological systems, such as within the human body. However, it may not fully represent the material's behavior in natural ecosystems. On the other hand, in their studies, Hou et al.<sup>[30]</sup> and Song et al.<sup>[32]</sup> employed papain and helicase enzymes, respectively, for conducting biodegradability assessments. Specifically, Hou et al. focused exclusively on the biodegradability of the dielectric layer, composed of glycerol and chitosan, while the biodegradability of the electrode material, a combination of copper nanowires (CuNW) and chitosan, was not evaluated. In the work of Song et al., whole sensor system was subjected to biodegradability testing and consequently electrode material (silver nanofibers) remained as residual waste. Consequently, the careful selection of materials and the methodology employed in our biodegradability testing demonstrate a superior approach compared to those documented

in the existing literature, highlighting the enhanced effectiveness and comprehensive scope of our study.

### 3. Conclusion

In conclusion, this research successfully demonstrates the development of an innovative, biodegradable, and edible wearable capacitive pressure sensor. Utilizing cellulose and pectin as main components, this sensor represents a significant advancement in sustainable electronics, addressing key environmental concerns associated with electronic waste. The sensor exhibits a range of desirable properties, including moderate sensitivity (0.0294 kPa<sup>-1</sup>), rapid response time (118 ms), and excellent durability over 10000 loading/unloading cycles. Its efficacy in real-time human motion detection applications further underscores its potential in various domains. The integration of green chemistry principles in the fabrication process, ensuring the absence of toxic chemicals, and the confirmed biodegradability of the sensor components enhance its environmental compatibility. This work not only contributes to the field of wearable electronics but also sets a precedent for future research in developing sustainable, high-performance electronic devices.

### 4. Experimental Section

**Materials:** Citrus peel-derived pectin, sodium chloride (NaCl, purity: 99%), calcium nitrate tetrahydrate (≥99%), graphite flakes (99% carbon, 100 mesh), and carnauba wax (No.1 yellow) were procured from Sigma-Aldrich. Sulphated cellulose nanocrystals were sourced from CelluForce. Common materials such as canola oil, medical-grade cellulose tape, and copper tape were obtained from local suppliers. Additionally, TEMPO-oxidized cellulose nanofibrils (CNF) with a concentration of 1.67% were secured from the Bioproducts Center at Aalto University.

Four distinct fungal strains were evaluated in biodegradability assessment study. *Aspergillus niger* NRRL 3 (*A. niger*) and *Trichoderma reesei* Rut C 30 (*T. reesei*) were sourced from our in-house culture repository. Additionally, *Absidia coerulea* DSM 3018 (*A. coerulea*) and *Gongronella butleri* DSM 2917 (*G. butleri*) were acquired from the Leibniz Institute DSMZ-German Collection of Microorganisms and Cell Cultures GmbH (DSMZ, Braunschweig, Germany). These strains were preserved in a state of spores/mycelia at –80 °C. Revival of the fungi was accomplished by culturing on potato dextrose agar (PDA) medium at 28 °C for a period of 7 days. Subsequent to this, spores were meticulously harvested under aseptic conditions and conserved at –80 °C in a 15% glycerol solution.

**Preparation of Cellulose Substrate:** A suspension of cellulose nanofiber (CNF) was prepared with a concentration of 0.5%, and it was subjected to continuous stirring overnight to assure homogeneous dispersion. To eliminate any bubbles formed within the suspension, a vacuum oven maintained at ambient temperature was utilized prior to the filtration process. Thereafter, the degassed suspension was transferred to the filtration apparatus, using a polyvinylidene fluoride (PVDF) membrane filter with a pore size of 0.45 μm. The resultant wet film was subsequently exposed to a hot press (Carver Inc., USA) treatment, conducted at a steady temperature of 50 °C for a fixed interval of 15 min.

**Fabrication of Carbon Cryogel Particles:** Cellulose nanocrystals were uniformly dispersed in deionized (DI) water, yielding a 4 wt% suspension. Following a sonication period of 30 min, a slow infusion of 100 mM calcium nitrate was introduced into the solution. The solution was then set aside overnight to enable comprehensive crosslinking, after which it was thoroughly rinsed with DI water to expel any residual salt. Post transformation into a cryogel via freeze-drying, it was positioned in a tubular furnace where it underwent a pyrolysis reaction lasting for 2 h at a temperature of

800 °C. The heating rate during this process was maintained at 5 °C/min, under a nitrogen-secured atmosphere.

**Preparation of Sensor Electrode:** An electrically conductive paste was prepared using the following methodology. Initially, a 0.1 g of carnauba wax and 0.3 g of canola oil was sequentially put into a 2 mL glass vial. This vial was then placed on a hot stirrer maintained at 100 °C and mixed until the carnauba wax had completely liquified. Subsequently, 0.04 g of carbon cryogel particles were gradually incorporated into the liquid mixture while gently stirring at a rate of 60 rpm. Following the cooling of the mixture to ambient temperature (RT), a quantity of 0.2 g paste was taken from the vial and placed on a cellulose substrate. This was accompanied by a heating phase at 100 °C until the paste was thoroughly liquefied. A Teflon sheet was then pressed to achieve a uniform coating. Lastly, it was left to cool down to RT.

**Fabrication of Pectin Xerogels:** Pectin powder was first dissolved in a 0.2 M NaCl aqueous solution, achieving a final concentration of 3 wt%. This mixture was stirred for a period of 24 h at RT. Subsequently, the solution was dispensed into a Teflon mold, which featured a copper plate at its base. The mold was then rested on the surface of dry ice, with a temperature of −79 °C, to facilitate the formation of freeze-casted gels. These gels were subjected to a submersion in cold ethanol, held at −15 °C, for a duration of three days. The first phase of solvent exchange was conducted in a mixture of ethanol and water in a 60/40 (v/v) ratio for a period of three days. During this stage, the solvent mixture was refreshed twice daily. Following this, a second phase of solvent exchange was carried out in acetone, continuing for an additional two days with a twice-daily replacement of fresh acetone. After completing the solvent exchange stages, the samples underwent a vacuum drying process. This was executed in a vacuum oven maintained at RT, resulting in the production of pectin xerogels.

**Preparation of the Pressure Sensors:** Pectin xerogel, measuring 1 mm in thickness cut along the ice growth direction, and cellulose films coated with carbon paste were precisely trimmed to dimensions of 2×2 cm. Following this, the pectin xerogel was carefully positioned in a sandwich-like configuration between two cellulose films, ensuring that the carbon paste-coated surfaces directly faced the pectin xerogel. Copper tape was subsequently affixed to the external surface of the cellulose films to establish electrical contact. As the final step in sensor assembly, a seal was created using medical-grade cellulose tape.

**Human Motion Detection Measurements:** The sensors were deliberately placed at designated points on the human body, encompassing areas like the elbow, knee, wrist, index finger joint, face, and underfoot. A porous and medically-approved elastic bandage was used to fasten the sensors securely at these locations. This bandage assisted in anchoring the sensors onto the specified muscle or joints. Concurrently with the articulation of the corresponding joints or muscles, the changes in capacitance were monitored, enabling an immediate evaluation of the sensor's real-time response to these movements. Written consent from all participants was obtained prior to the research (Aalto University Research Ethics Committee with D/1302/03.04/2022 WEARSENSNANO decision number).

**Biodegradability Assessment:** In our study, a liquid culture biodegradability assay method was employed to assess the biodegradability of sensor components, including a cellulose substrate, carbon cryogel paste, and pectin xerogel. The experiment was executed using 16 mm sterile glass test tubes. Each tube, containing 5 ml of the minimal medium without glucose (6.7 g/L Yeast nitrogen base (YNB) with ammonium sulfate without amino acids, pH 5.8), was introduced to a small segment of the test material. Subsequently, 10 µL of the respective fungal spore suspension was added. The tubes were then incubated at 30 °C with an agitation rate of 220 rpm for a span of 10 weeks. Two controls were set up: Control 1, containing only the test material in the minimal medium, and Control 2, with the minimal medium introduced solely to fungal spores. Periodic, weekly photographic records were made. As and when required, the well's volume was restored to nearly its original measurement using a YNB medium, both to replenish essential nutrients and to account for evaporative losses.

**Characterization:** The morphological characterization was performed using a scanning electron microscope (SEM, Tescan Mira3). The capacitance values of the sensors were measured using an LCR meter (E4980AL, KEYSIGHT) with an applied AC voltage of 1 V and a frequency of 10 kHz.

External pressure was applied to the sensors using a mechanical tester equipped with a computer-controlled stage (TA.XTplus, Stable Micro Systems). The determination of response and recovery times was performed with OriginLab Pro software via utilization of the Rise Time Gadget for this purpose. To ensure precision in measuring these times and to reduce discrepancies related to signal transition corners, the times were defined as the period spanning from 10% to 90% of the total amplitude.

The resistance values ( $R$ ) of the carbon paste electrodes were measured using a digital multimeter. Resistivity ( $\rho$ ) of the carbon paste was calculated considering the described geometry through the equation:

$$\rho = R \cdot \frac{W \cdot t}{L} \quad (2)$$

where  $\rho$ ,  $W$  (2.5 cm),  $t$  (50 µm) and  $L$  (2.5 cm) denotes resistivity, width, thickness, and length, respectively. I-V curves were obtained using a parametric analyzer (Keithley 4200A-SCS Clarius).

**Statistical Analysis:** Resistivity and thickness of the samples were measured over three identical samples for each data-point, and data was presented as average and standard deviation (Table S1, Supporting Information). Sensor performance tests (Figure 3) and human motion detection (Figures 4 and S7 and S8, Supporting Information) characterizations were performed with one sample. All the data analyses were carried out using Matlab and Excel.

## Supporting Information

Supporting Information is available from the Wiley Online Library or from the author.

## Acknowledgements

This research was funded by the H2020-MSCA-IF-2020 with a grant number of 101031327 (WEARSENSNANO) as well as by the ERC StG project 949648 “ModelCom”. Y.A.H. acknowledges the funding from the Academy of Finland's Flagship Programme under Projects No. 318890 and 318891 (Competence Center for Materials Bioeconomy, FinnCERES).

## Conflict of Interest

The authors declare no conflict of interest.

## Data Availability Statement

The data that support the findings of this study are available from the corresponding author upon reasonable request.

## Keywords

biodegradable sensor, capacitive pressure sensor, edible sensor, human motion detection, wearable sensor

Received: February 23, 2024  
Revised: July 8, 2024  
Published online: August 8, 2024

- [1] T. Q. Trung, N.-E. Lee, *Adv. Mater.* **2016**, *28*, 4338.
- [2] R. B. Mishra, N. El-Atab, A. M. Hussain, M. M. Hussain, *Adv. Mater. Technol.* **2021**, *6*, 2001023.

- [3] Q. Shu, Y. Pang, Q. Li, Y. Gu, Z. Liu, B. Liu, J. Li, Y. Li, *J. Mater. Chem. A* **2024**, *12*, 9296.
- [4] C. Zhi, S. Shi, Y. Si, B. Fei, H. Huang, J. Hu, *Adv. Mater. Technol.* **2023**, *8*, 2201161.
- [5] X. Xiong, J. Liang, W. Wu, *Nano Energy* **2023**, *113*, 108542.
- [6] B. Hou, L. Yi, C. Li, H. Zhao, R. Zhang, B. Zhou, X. Liu, *Nat. Electron.* **2022**, *5*, 682.
- [7] L. Burnie, N. Chockalingam, A. Holder, T. Claypole, L. Kilduff, N. Bezodis, *Foot* **2023**, *56*, 102046.
- [8] K.-H. Ha, H. Huh, Z. Li, N. Lu, *ACS Nano* **2022**, *16*, 3442.
- [9] X. Wang, J. Yu, Y. Cui, W. Li, *Sens. Actuators A Phys.* **2021**, *330*, 112838.
- [10] F. Basarir, Z. Madani, J. Vapaavuori, *Adv. Mater. Interfaces* **2022**, *9*, 2200866.
- [11] C. Gu, S. Chen, X. Guo, In *The 8th Annual IEEE International Conference on Nano/Micro Engineered and Molecular Systems*, IEEE, New York, **2013**, pp. 1183.
- [12] Y. Cheng, R. Wang, H. Zhai, J. Sun, *Nanoscale* **2017**, *9*, 3834.
- [13] B. Zhang, Z. Xiang, S. Zhu, Q. Hu, Y. Cao, J. Zhong, Q. Zhong, B. Wang, Y. Fang, B. Hu, J. Zhou, Z. Wang, *Nano Res.* **2014**, *7*, 1488.
- [14] W. Hu, X. Niu, R. Zhao, Q. Pei, *Appl. Phys. Lett.* **2013**, *102*, 83303.
- [15] W. Yang, N.-W. Li, S. Zhao, Z. Yuan, J. Wang, X. Du, B. Wang, R. Cao, X. Li, W. Xu, Z. L. Wang, C. Li, *Adv. Mater. Technol.* **2018**, *3*, 1700241.
- [16] P. Wang, G. Li, J. Liu, Z. Hou, C. Meng, S. Guo, C. Liu, S. Fan, *Adv. Mater. Interfaces* **2021**, *8*, 2100998.
- [17] S. Pyo, Y. Eun, J. Sim, K. Kim, J. Choi, *Micro Nano Syst. Lett.* **2022**, *10*, 9.
- [18] Y. Zhou, D. Dai, Y. Gao, Z. Zhang, N. Sun, H. Tan, X. Cai, J. Cai, *Chem-NanoMat.* **2021**, *7*, 982.
- [19] Q.-T. Lai, X.-H. Zhao, Q.-J. Sun, Z. Tang, X.-G. Tang, V. A. L. Roy, *Small* **2023**, *19*, 2300283.
- [20] W. Li, L. Xiong, Y. Pu, Y. Quan, S. Li, *Nanoscale Res. Lett.* **2019**, *14*, 183.
- [21] S. Yao, Y. Zhu, *Nanoscale* **2014**, *6*, 2345.
- [22] X. Shuai, P. Zhu, W. Zeng, Y. Hu, X. Liang, Y. Zhang, R. Sun, C. Wong, *ACS Appl. Mater. Interfaces* **2017**, *9*, 26314.
- [23] Y. Wan, Z. Qiu, Y. Hong, Y. Wang, J. Zhang, Q. Liu, Z. Wu, C. F. Guo, *Adv. Electron. Mater.* **2018**, *4*, 1700586.
- [24] Y. Joo, J. Byun, N. Seong, J. Ha, H. Kim, S. Kim, T. Kim, H. Im, D. Kim, Y. Hong, *Nanoscale* **2015**, *7*, 6208.
- [25] V. Forti, C. P. Balde, R. Kuehr, G. Bel, *The Global E-waste Monitor 2020: Quantities, flows and the circular economy potential*, Bonn/Geneva/Rotterdam, xx xx, **2020**.
- [26] J. Zhu, H. Wen, H. Zhang, P. Huang, L. Liu, H. Hu, *Sustain. Mater. Technol.* **2023**, *35*, e00530.
- [27] C. M. Boutry, A. Nguyen, Q. O. Lawal, A. Chortos, S. Rondeau-Gagné, Z. Bao, *Adv. Mater.* **2015**, *27*, 6954.
- [28] C. M. Boutry, Y. Kaizawa, B. C. Schroeder, A. Chortos, A. Legrand, Z. Wang, J. Chang, P. Fox, Z. Bao, *Nat. Electron.* **2018**, *1*, 314.
- [29] M. A. U. Khalid, M. Ali, A. M. Soomro, S. W. Kim, H. B. Kim, B.-G. Lee, K. H. Choi, *Sensors Actuators A Phys.* **2019**, *294*, 140.
- [30] C. Hou, Z. Xu, W. Qiu, R. Wu, Y. Wang, Q. Xu, X. Y. Liu, W. Guo, *Small* **2019**, *15*, 1805084.
- [31] A. Elsayes, V. Sharma, K. Yiannacou, A. Koivikko, A. Rasheed, V. Sariola, *Adv. Sustain. Syst.* **2020**, *4*, 2000056.
- [32] Z. Song, Z. Liu, L. Zhao, C. Chang, W. An, H. Zheng, S. Yu, *Org. Electron.* **2022**, *106*, 106539.
- [33] N. Fumeaux, D. Briand, *npj Flex. Electron.* **2023**, *7*, 14.
- [34] I. K. Ilic, V. Galli, L. Lamanna, P. Cataldi, L. Pasquale, V. F. Annese, A. Athanassiou, M. Caironi, *Adv. Mater.* **2023**, *35*, 2211400.
- [35] J. Kim, I. Jeerapan, B. Ciui, M. C. Hartel, A. Martin, J. Wang, *Adv. Healthcare Mater.* **2017**, *6*, 1700770.
- [36] Y. Wu, D. Ye, Y. Shan, S. He, Z. Su, J. Liang, J. Zheng, Z. Yang, H. Yang, W. Xu, H. Jiang, *Adv. Mater. Technol.* **2020**, *5*, 2000100.
- [37] I. K. Ilic, L. Lamanna, D. Cortecchia, P. Cataldi, A. Luzio, M. Caironi, *ACS Sens.* **2022**, *7*, 2995.
- [38] L. Lamanna, P. Cataldi, M. Friuli, C. Demitri, M. Caironi, *Adv. Mater. Technol.* **2023**, *8*, 2200731.
- [39] V. F. Annese, P. Cataldi, V. Galli, G. Coco, J. P. V. Damasceno, A. Keller, Y. Kumaresan, P. Rossi, I. K. Ilic, B. Kwak, L. T. Kubota, A. Athanassiou, J. Rossiter, D. Floreano, M. Caironi, *Adv. Sens. Res.* **2024**, *3*, 2300150.
- [40] A. S. Sharova, F. Melloni, G. Lanzani, C. J. Bettinger, M. Caironi, *Adv. Mater. Technol.* **2021**, *6*, 2000757.
- [41] K. Fukada, T. Tajima, K. Hayashi, *ACS Appl. Electron. Mater.* **2022**, *4*, 6087.
- [42] P. Cataldi, L. Lamanna, C. Bertei, F. Arena, P. Rossi, M. Liu, F. Di Fonzo, D. G. Papageorgiou, A. Luzio, M. Caironi, *Adv. Funct. Mater.* **2022**, *32*, 2113417.
- [43] F. Zou, H. Li, Y. Dong, G. C. Tewari, J. Vapaavuori, *Chem. Eng. J.* **2022**, *439*, 135738.
- [44] T. Xu, W. Wang, X. Bian, X. Wang, X. Wang, J. K. Luo, S. Dong, *Sci. Rep.* **2015**, *5*, 12997.
- [45] D. Zenkert, A. Shipsha, M. Burman, *J. Sandw. Struct. Mater.* **2006**, *8*, 517.
- [46] S. Li, Y. Zhang, Y. Wang, K. Xia, Z. Yin, H. Wang, M. Zhang, X. Liang, H. Lu, M. Zhu, H. Wang, X. Shen, Y. Zhang, *InfoMat* **2020**, *2*, 184.
- [47] R. H. Bischof, J. Ramoni, B. Seiboth, *Microb. Cell Fact.* **2016**, *15*, 106.
- [48] I. S. Druzhinina, C. P. Kubicek, *Adv. Appl. Microbiol.* **2016**, *95*, 69.
- [49] P. M. Coutinho, M. R. Andersen, K. Kolenova, P. A. vanKuyk, I. Benoit, B. S. Gruben, B. Trejo-Aguilar, H. Visser, P. van Solingen, T. Pakula, B. Seiboth, E. Battaglia, G. Aguilar-Osorio, J. F. de Jong, R. A. Ohm, M. Aguilar, B. Henrissat, J. Nielsen, H. Stålbrand, R. P. de Vries, *Fungal Genet. Biol.* **2009**, *46*, S161.
- [50] E.-S. A. Kassim, *Microbiol. Immunol.* **1982**, *26*, 449.
- [51] A. Patyshakuliyeva, M. Arentshorst, I. E. Allijn, A. F. J. Ram, R. P. de Vries, I. B. Gelber, *Biotechnol. Lett.* **2016**, *38*, 969.
- [52] R. Valsalan, D. Mathew, G. Devaki, *J. Genet. Eng. Biotechnol.* **2022**, *20*, 74.
- [53] R. Abdullah, A. Jafer, K. Nisar, A. Kaleem, M. Iqtedar, T. Iftikhar, F. Saleem, S. Naz, *Biosci. J.* **2018**, *34*, 1025.
- [54] A. M. Khattab, in *Pectins - The New-Old Polysaccharides* (Ed: A. Masuelli), IntechOpen, Rijeka **2022**, Ch. 5.
- [55] E. S. Martens-Uzunova, P. J. Schaap, *Fungal Genet. Biol.* **2009**, *46*, S170.
- [56] L. Gao, G. Liu, Q. Zhao, Z. Xiao, W. Sun, X. Hao, X. Liu, Z. Zhang, P. Zhang, *Carbohydr. Polym.* **2022**, *297*, 120025.
- [57] N. A. Hamdi, S. Sha'arani, N. F. Azman, S. B. M. Rafi, E. Norsin, N. Othman, *IOP Conf. Ser. Earth Environ. Sci.* **2022**, *1091*, 012054.
- [58] T. A. de Oliveira, I. de Oliveira Mota, F. E. P. Mousinho, R. Barbosa, L. H. de Carvalho, T. S. Alves, *J. Appl. Polym. Sci.* **2019**, *136*, 48240.